

# Functional alignment with anatomical networks is associated with cognitive flexibility

John D. Medaglia<sup>1,2</sup>, Weiyu Huang<sup>3</sup>, Elisabeth A. Karuza<sup>4</sup>, Apoorva Kelkar<sup>1</sup>, Sharon L. Thompson-Schill<sup>4</sup>, Alejandro Ribeiro<sup>3</sup> and Danielle S. Bassett<sup>3,5\*</sup>

**Cognitive flexibility describes the human ability to switch between modes of mental function to achieve goals. Mental switching is accompanied by transient changes in brain activity, which must occur atop an anatomical architecture that bridges disparate cortical and subcortical regions via underlying white matter tracts. However, an integrated understanding of how white matter networks might constrain brain dynamics during cognitive processes requiring flexibility has remained elusive. Here, to address this challenge, we applied emerging tools from graph signal processing to examine whether blood oxygen level-dependent signals measured at each point in time correspond to complex underlying anatomical networks in 28 individuals performing a perceptual task that probed cognitive flexibility. We found that the alignment between functional signals and the architecture of the underlying white matter network was associated with greater cognitive flexibility across subjects. By computing a concise measure using multi-modal neuroimaging data, we uncovered an integrated structure-function relation of human behaviour.**

Cognitive flexibility is involved in virtually every complex behaviour from mental arithmetic to processing of visual stimuli. For example, when navigating complex environments, humans can flexibly switch between two foci of attention or between two processing modalities in order to effectively respond to sensory inputs. Although it is a hallmark of human cognition, flexible switching is also associated with a measurable cost: moving from one task to another induces a natural extension in the time it takes a person to respond to stimuli<sup>1</sup>. In patients with neurological syndromes, this cost is even greater, to the point where it can hamper a patient's ability to engage in the basic activities of daily living<sup>2</sup>, impacting long-term cognitive outcomes<sup>3</sup>. In healthy individuals, cognitive flexibility varies considerably, and individual differences in this trait contribute to mental facets ranging from the development of reasoning ability<sup>4</sup> to quality of life in late age<sup>5</sup>. Clarifying the nature of cognitive flexibility in the human brain is critical to understand the human mind.

The physiological origins of cognitive flexibility are thought to lie in corticobasal ganglia-thalamocortical loops<sup>6</sup>: regions of the fronto-parietal and cingulo-opercular systems are activated by cognitive switching tasks<sup>7–10</sup>. In switching paradigms, the anterior cingulate is thought to contribute negative feedback detection following switches<sup>11</sup>, whereas the lateral prefrontal cortex maintains rules and inhibits incorrect responses<sup>12</sup> and the medial parietal lobes contribute to shifts in spatial attention, working memory and categorization rules<sup>13</sup>. All of these regions anatomically connect to subcortical regions, which are postulated to mediate processes that both suppress prepotent motor responses and transition between behavioural outputs to meet task goals<sup>14</sup>. Interactions between cortical systems and motor outputs are thought to be anatomically mediated by subcortical circuits<sup>7,9,15–17</sup>. However, understanding exactly how this circuit supports task switching has remained challenging, particularly because it requires the integration of regional activity,

inter-regional anatomical connectivity and observable measures of behaviour. Whereas regional activity and behavioural markers of cognitive flexibility are relatively straightforward to estimate, it is less straightforward to integrate these features with the white matter structure (the connectome<sup>18</sup>) that guides the propagation of functional signals<sup>19–21</sup>.

Given the complex and diverse neurobiology involved in cognitive control, frameworks that include a concise correspondence between brain network structure, function and cognitive measures have the potential to produce more comprehensive understanding of human cognition<sup>22,23</sup>. Conceptually, underlying white matter network organization in the brain physically mediates communication among brain regions. However, analytic frameworks that explicitly use white matter structure to constrain cognitively relevant functional signals are lacking. Such approaches may allow investigators to assign the relative contributions of well-described systems in the brain<sup>8,24</sup> to specific cognitive variables by integrating neurophysiological dynamics and anatomy.

To address this challenge, we aimed to identify the multimodal integration of network anatomy and functional signals that support cognitive switching. Here, we introduce an approach that allows us to examine the distinct contributions of functional signals in the context of anatomically linked regions in human brain networks. In a cohort of 28 healthy adult human subjects, we collected diffusion spectrum imaging (DSI) data as well as blood oxygen level-dependent (BOLD) functional magnetic resonance imaging (fMRI) data acquired during the performance of a cognitive switching paradigm based on a set of shapes that could be perceived as composed of different features at the local versus global scales<sup>25</sup> (see Fig. 1). From the DSI data, we constructed anatomical brain networks in which 111 cortical, subcortical and cerebellar regions<sup>26,27</sup> were linked pairwise by the density of streamlines reconstructed by a tractography algorithm. Next, we used the eigenspectrum of these anatomical

<sup>1</sup>Department of Psychology, Drexel University, Philadelphia, PA, USA. <sup>2</sup>Department of Neurology, Perelman School of Medicine, University of Pennsylvania, Philadelphia, PA, USA. <sup>3</sup>Department of Electrical and Systems Engineering, University of Pennsylvania, Philadelphia, PA, USA. <sup>4</sup>Department of Psychology, University of Pennsylvania, Philadelphia, PA, USA. <sup>5</sup>Department of Bioengineering, University of Pennsylvania, Philadelphia, PA, USA.

\*e-mail: [dsb@seas.upenn.edu](mailto:dsb@seas.upenn.edu)

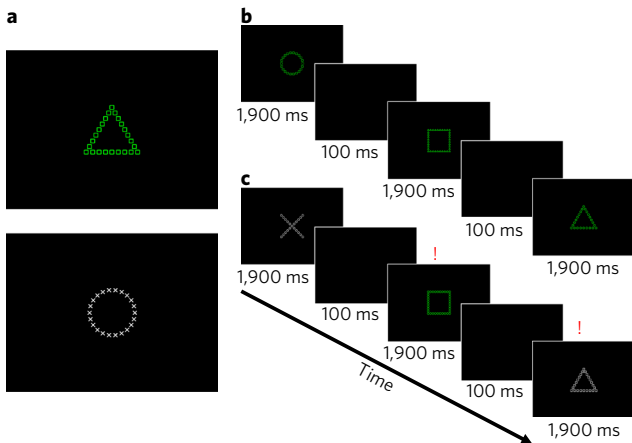


**Fig. 1 | Cognitive task requiring perceptual switching.** **a**, Example stimuli based on Navon local-global features. Subjects were trained to respond to the larger (or global) shape if the stimulus was green and to the smaller (or local) shape if it was white. **b**, An example of the non-switching condition for responses. Subjects viewed a sequence of images and were instructed to respond as quickly and accurately as possible. **c**, An example of the switching condition between stimuli requiring global and local responses. Here, trials with a red exclamation point are switches from the previous stimulus.

networks to measure the relative separation of framewise BOLD signals across brain regions (see Fig. 2 and Methods). Specifically, each regional signal was decomposed into a proportion that aligned well with the anatomical network (aligned) and a proportion that did not align tightly with the network (liberal; see Fig. 3 for a schematic example of these types of signals). Intuitively, alignment and liberality measured different amounts of signal deviation from the underlying anatomical network.

To define these measures, we used a generalization of the traditional Fourier transform for time-series analysis to the graph domain using a graph Fourier transform (GFT)<sup>28</sup>, which can quantify the way in which signals are organized atop an underlying graph. In conventional frequency analysis using the Fourier transform, low frequency components represent time series that vary slowly over time, whereas high frequency components denote time series that vary rapidly over time. In graph frequency analysis using GFT, aligned components represent signals that vary smoothly across the graph, whereas liberal components denote signals that vary highly across the graph at single moments in time. Because we used GFT for the BOLD measurements at each time point instead of across time points, this technique identifies where and to what extent BOLD signals across the brain are organized in a manner that is aligned with white matter networks. Conceptually, this technique allowed us to identify to what degree individual BOLD signals deviate weakly versus strongly from the underlying white matter anatomy. Just as a single brain region can display a time series with both low and high frequency components, so too can a single brain region display both aligned and liberal components (see Fig. 4 for a schematic representation of the distinction between time Fourier transformation and GFT).

We anticipated that functional alignment with anatomical networks is an individually variable feature that facilitates cognitive flexibility. Whereas previous studies have focused on region-specific mechanisms associated with this process, our approach allowed us to examine the role of local neural processes across the brain's distributed anatomical network. We hypothesized that moment-to-moment alignment in human brain networks facilitates switching performance, measured by switch costs, indicating inter-individual variability in the degree of organization of information

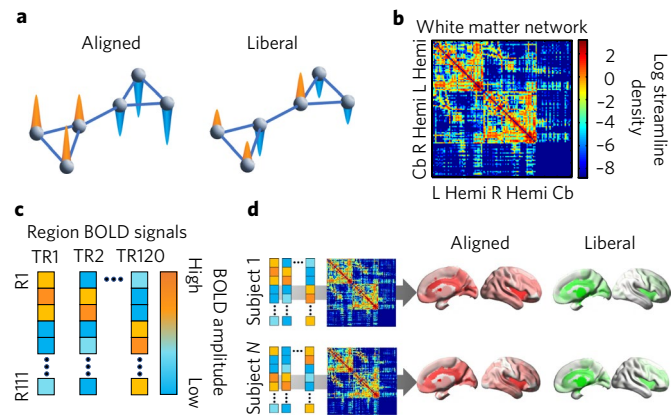


**Fig. 2 | Multimodal approach to the study of cognitive switching using emerging graph signal processing tools.** **a**, A notion of signal independence on a schematic modular network. Left: an aligned signal on top of a given graph is one in which the magnitude of functional signals, represented by the directionality of the coloured cones, corresponds tightly to that expected by the network's organization. In this example, one cluster of nodes contains similar positive signals, and the other cluster contains similar negative signals. Right: a liberal signal on top of a given graph is one in which signals diverge significantly from the underlying network. **b**, For each of the 28 subjects, a white matter graph (a weighted adjacency matrix including white matter streamlines) is constructed from 111 anatomically defined regions where connections are the streamline density between region pairs. Cb, cerebellum; Hemi, hemisphere; L, left; R, right. **c**, From BOLD fMRI data acquired during the performance of the Navon task, we extract regional mean time series, which we treated as graph signals. R, region; TR, repetition time. **d**, For each subject, graph signals were decomposed into aligned and liberal components using the underlying eigenspectrum of the white matter graph. Aligned and liberal signals were mapped to the nodes in the brain, and we estimated the correlation between the relative alignment (or liberality) and the switch costs estimated from behavioural performance on the task. See Methods for details.

processing by the topology of underlying anatomy. Our switching task presumably involved proactive control—sustained and anticipatory maintenance of goal-relevant information—and reactive control—transient, stimulus-driven goal reactivation<sup>29</sup>. In proactive switching, activation in the lateral prefrontal cortex is thought to be associated with maintaining task goals, whereas reactive control may be associated with a more transient activation of lateral prefrontal cortex and a broader network of corticobasal ganglia mechanisms interacting with the pre-supplementary motor area, and anterior cingulate cortex<sup>29</sup>. In this ‘dual mechanisms of control’ framework, both processes may be semi-independent and engaged simultaneously, and normative human function may represent a balance between these modes<sup>29</sup>. However, the representation of these modes of function is incompletely understood in human brain networks, calling for a need to focus on the joint contributions of anatomical and functional network properties that support effective cognitive control<sup>8,30</sup>.

We hypothesized that we could identify anatomy-aligned functional signals in the brain that potentially represent efficiently organized signals with respect to anatomy, in addition to liberal signals that do not correspond to the inherent organization of underlying white matter networks. In our approach, four distinct possibilities existed dependent on the signal type. As such, it was possible that increasing or relaxing the alignment of the most aligned signals was associated with better performance or that increasing or relaxing the liberality of the most liberal signals was associated with better performance. Among these possibilities, we anticipated that variation in liberality of the most liberal signals—those signals which deviate

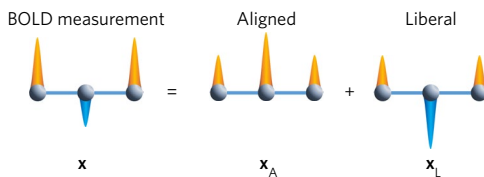


**Fig. 3 | Signal decomposition into anatomy.** BOLD signals are decomposed into aligned and liberal signal components. Left side of the equation: a schematic BOLD signal on a simple anatomical network. Here, two signals are stronger in the high direction than in the low direction. Right side of the equation: the signals across the network are decomposed into an aligned and liberal component. The original signals can be reconstructed from a basis set including a weighted part of the signal that is aligned with the anatomical network and another part that is liberal with respect to the anatomical network. Variable names indicate the following:  $x$ , the original BOLD signal measurements;  $x_A$ , the part of the original BOLD signal that is aligned with anatomy;  $x_L$ , the part of the original BOLD signal that is liberal with respect to anatomy.

greatly from anatomical expectations—would be most strongly correlated with cognitive switching. This hypothesis is built on the fact that the rules learned in our cognitive switching tasks are learned shortly before performing the task, and are therefore unlikely to be represented in changes in long-distance white matter pathways. Flexible functional deviations in white matter organization may therefore be associated with efficient switching. However, it was possible that either increasing or decreasing liberality would be associated with better performance. In the case of increasing liberality, a particularly anatomy-divergent signal organization may have contributed to cognitive flexibility. In the case of decreasing liberality, modest alignment among liberal signals may have provided beneficial organization that efficiently supports cognitive flexibility. To discriminate between these possibilities, our method allowed us to examine whether structure and function operate synergistically or divergently to promote cognitive performance. We additionally examined the relationship between signal alignment and other related behavioural measures—inhibition and working memory—using a Stroop paradigm and working memory task (for brevity, references to Supplementary Tables for these two tasks are mentioned in the main text where relevant).

## Results

**BOLD signal alignment concentrations across the brain.** We observed that aligned signals were concentrated within default mode, fronto-parietal, cingulo-opercular and subcortical systems across subjects, whereas the liberal signals were concentrated largely in the subcortical system (Fig. 5). The significance of these concentrations within systems was confirmed statistically using a non-parametric permutation test ( $\alpha=0.05$ ) in which we shuffled the values of alignment (or liberality) uniformly at random across brain regions before computing the mean alignment (or liberality) value within each system<sup>31</sup>.

Interestingly, we observed that the insula, anterior cingulate and subcortical systems shared both aligned and liberal signals, indicating that the content of BOLD signals in these areas are complex with respect to underlying anatomy. The values of both alignment and liberality were significantly greater than expected in these structures. Other regions across the brain expressed relatively lower amounts of both of these properties. By separating the signal components across regions, we were able to identify potentially behaviourally sensitive proportions of signals occurring atop anatomical networks. To see results from an analysis of the spatial correspondence between aligned and liberal signals in the current dataset, see Supplementary Information.

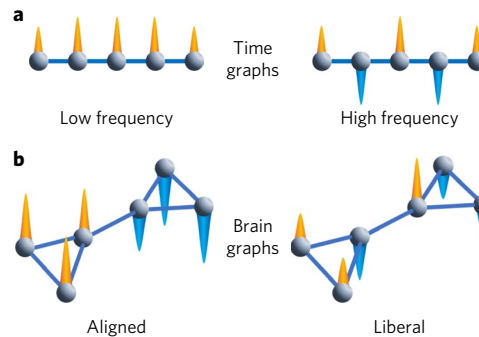


**Fig. 4 | Signal frequency in the time domain versus alignment in the graph domain.** **a**, A simple graph can represent a signal process in time. Imagine that the nodes in the graph are moments in time, and the edges between nodes represent links between adjacent moments in time. The image on the left then represents a low frequency signal process in which the orange cones represent positive signals that do not vary significantly with respect to the time dimension. The image on the right represents a high frequency signal process in which the orange cones represent positive signals and the blue cones represent negative signals. The signals flip from moment to moment, which is the basis of a high frequency signal. A traditional Fourier analysis on real signals can separate both high and low frequency activity observed in a single set of nodes (moments in time). **b**, We can extend this notion directly to more complex graph structures, such as those observed in human brain networks with the GFT. As in the time graph in **a**, we observe nodes, edges and a signal at each node. Unlike the time graph, which constitutes a linear ordering of connected nodes, the more complex graph may have modules and other mesoscale features. On the left, we observe an aligned signal: the signals in nodes that highly connect to one another exhibit similar signals to one another. On the right, the signal is liberal with respect to the underlying graph: the signals in nodes that highly connect to one another do not exhibit similar signals to one another. In real signals, such as BOLD signals observed at a single moment in time, each node can contribute signals that may be to some extent aligned and to some extent liberal.

**Associations between BOLD signal alignment and cognitive switch costs.** Next, we calculated the correlation between aligned and liberal BOLD signals across the brain and cognitive switch costs (response times during trials with a colour-cued switch versus non-switch trials). We observed that variability in aligned signals was not associated with switch costs ( $R=0.15$ ,  $P=0.43$ , accounting for 2% of the variance), whereas variability in liberal signals accounted for 32% of the variance ( $R=0.57$ ,  $P=0.002$ ; see Fig. 6). Using aligned signals as covariates in a partial correlation analysis between liberality and switch costs revealed that the correlation remained significant ( $R=0.55$ ,  $P=0.002$ ). Among the liberal signals, lower values of liberality (that is, relative alignment) were also associated with lower switch costs during both fixation ( $R=0.62$ ,  $P=0.0006$ ) and non-switching ( $R=0.71$ ,  $P=0.0001$ ) perceptual blocks.

These results demonstrate that relative BOLD signal alignment among liberal signals with anatomy was associated with greater cognitive flexibility, a finding that highlights the importance of simultaneously considering both functional and anatomical neuroimaging in the study of higher-order cognitive processes. This indicates that behaviourally relevant signals can be dissociable in the graph domain even when the same regions partially contribute to both types of signals. Liberal signals were specifically related to cognitive switching as opposed to performance more generally during the Navon task. We found that the liberal signals in all blocks were correlated with response times during trials that occurred during switching blocks as well as switch costs. Liberal signals were not correlated with performance on the non-switching blocks,

suggesting that these signals are specifically related to cognitive control demands introduced during the switching condition relative to the non-switching condition (see Supplementary Tables 1–4).

**The specificity of BOLD signal alignment in cognitive control.** The fact that statistically significant relationships could be found between switching performance and the signals calculated in the Navon fixation, non-switching and switching blocks suggests that liberal signal organization is a stable variable in the context of the Navon task (see Supplementary Information). Thus, testing whether liberal signals are specifically relevant during the switching task relative to other cognitive control processes, such as inhibition and working memory, is crucial. In additional analyses, covarying for Stroop performance did not reduce the correlations between liberality during the Navon task and switching behaviour (see Supplementary Tables 17, 18). Moreover, we find that BOLD liberality observed in the same subjects during fixation periods between Stroop inhibition task blocks does not correlate with cognitive switching performance (see Supplementary Tables 21, 22). Finally, no relationship between BOLD signal alignment and working memory performance was observed in an independent sample from the Human Connectome Project (see Supplementary Tables 27–30).

## Discussion

Taken together, these findings indicate that the liberality–switching relationship was specific to the Navon task and not accounted for by cognitive inhibition or working memory, providing evidence of a sensitive and specific brain–behaviour relationship. Overall, these findings may indicate that some brains are at a natural advantage to meet switching demands, and that switching-specific relationships between signal and anatomy can be detected when task demands necessitate preparedness for cognitive switches. Given the persistence of the liberality signal across task blocks, the current study is compatible with the notion that these signals exist throughout the task, potentially representing proactive cognitive control. Future event-related studies could determine whether liberal versus aligned signals are associated with the proactive or reactive aspects of control in cognitive switching.

In some theoretical accounts of cognitive control, we might expect that performance is facilitated by associations between stimulus features that could have arisen from practice<sup>32</sup>, and the neuroplastic changes that facilitate such learned associations could have effects at scales detectable with diffusion imaging<sup>33–36</sup>. In that case, one possibility is that greater reliance on these pathways (for example, measured here as the highly aligned BOLD signal component) would be facilitative of better performance, potentially representing reliance on well-learned information when performing cognitive switches. However, the rules for the current Navon task were learned shortly before performance, perhaps limiting the use of overlearned representations and emphasizing the neural processing represented by the liberal BOLD signals. Nevertheless, relative alignment of the liberal BOLD signals with white matter anatomy was associated with better performance, suggesting that even in the context of a recently learned task, increased functional reliance on white matter network organization is advantageous for performance. While speculative, future studies could test whether a dissociation exists between overlearned and newly learned tasks and whether the effect observed here generalizes to other recently learned switching tasks. Such studies could provide intuition for the neuroanatomical expression of the interplay between learning at short versus long timescales and cognitive control.

These findings complement previous studies of executive function that have focused on node-level, edge-level and module-level features of brain networks<sup>16,37</sup>. Here, we examined brain function as a series of time-evolving states<sup>31,38</sup> that were organized in relation to the underlying pattern of white matter tracts. The state-based

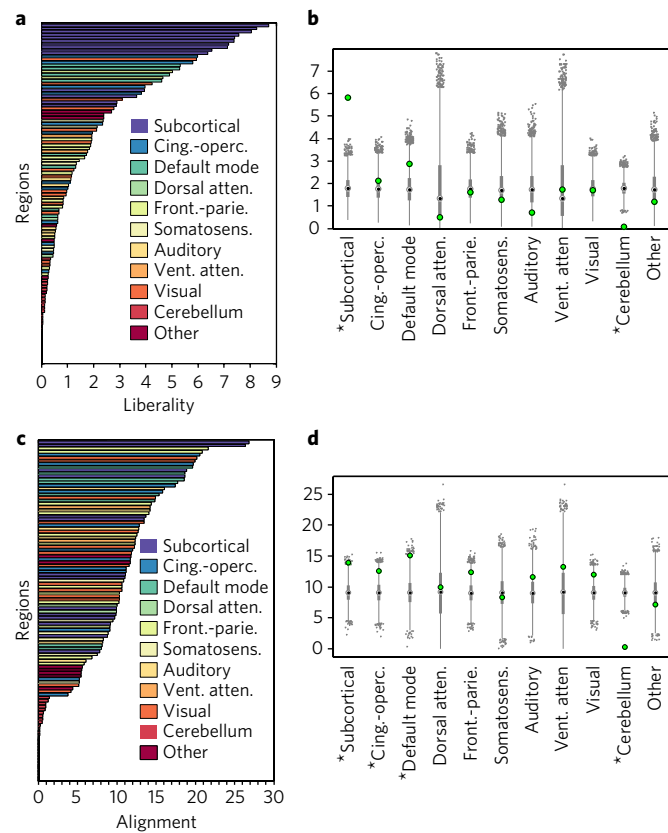


**Fig. 5 | Non-parametric permutation test for signal concentration within cognitive systems.** **a**, For the 28 subjects, the liberal signal concentrations sorted from highest (top) to lowest (bottom) concentration across all regions. **b**, Liberal signals are most concentrated in subcortical regions. **c**, Aligned signal concentrations sorted from highest (top) to lowest (bottom) concentration across all regions in all 28 subjects. **d**, Aligned signals are most concentrated in fronto-parietal, cingulo-opercular, default mode and subcortical systems. The bars in **a** and **c** represent the mean signal liberality or alignment in the 111 regions colour-coded by their system assignment. The x axes represent the GFT signal values for each region, where increasing values represent more liberality in **a** and more alignment in **c**. In panels **b** and **d**, the grey bars represent the 25th and 75th percentiles of the values in the null permutations, the grey whiskers extend to the most extreme data points not considered outliers, and the grey dots represent outliers in the permutation distributions. The green dot represents the observed value for the system. An asterisk indicates a statistically significant signal concentration in the system relative to the null distribution in the permutation test (\* $P < 0.05$ ). Cing.-operc, cingulo-opercular; atten., attention; front.-parie., fronto-parietal; somatosens., somatosensory; vent., ventral.

focus of our approach also offers insights into the differential extent to which specific cognitive systems deviate from tract anatomy, underscoring anatomical contributions to the organization of brain dynamics across subjects. It also allowed us to examine the complexity in BOLD signals that is not evident in functional connectivity analyses computed over time<sup>39</sup>. Because functional connectivity in fMRI is typically computed over many BOLD time points, our approach characterizes the organization of the elements that constitute common functional connectivity measures.

Our results contextualize previous models of corticostriatal cognitive switching mechanisms<sup>14,40</sup> within a connectomic perspective. As a complement to previous findings implicating individual prefrontal, parietal and striatal systems in cognitive switching, our

results highlight the importance of anatomical network organization, and the central role of subcortical functional dynamics atop that structure. This observation is particularly noteworthy in the context of prior studies, which showed that subcortical and anterior cingulate regions manage multiple inputs and outputs among cortical systems during task transitions<sup>9,41</sup>, potentially requiring more diverse signal organization relative to anatomical networks. In addition, a high convergence of weak liberal and aligned signals was observed in the cerebellum, complementing the high convergence of strong liberal and aligned signals in the cingulate and subcortical regions, which are thus responsible for most of the behavioural variance in our analysis (see Supplementary Tables 9, 10). Notably, cerebellar architecture has a tenfold greater neural density than other regions in the brain<sup>42</sup> with distinctive neural dynamics; thus, our approach may not be sensitive to cerebellar signaling properties thought to contribute to higher cognitive function<sup>43</sup>, which could form a focus for future research involving measurements of neural spike trains and cerebellar microcircuitry.

Our approach also adds a critical perspective to broader interests in the relationship between brain network anatomy and function. Previous reports have established relationships between anatomical networks and functional connectivity<sup>20,44–48</sup>. The information content in BOLD correlations computed over long time series is relatively low<sup>39</sup>. Our current work applied an altogether distinct approach to this problem by linking anatomy, function, and cognition. The time repetition-wise analysis is similar to studies of BOLD signal amplitude in cognitive conditions, which has formed a backbone of cognitive neuroscience research since the invention of fMRI. Specifically, the alignment measure was based on the distribution of BOLD signal amplitudes across brain regions at single time points in different cognitive conditions, rather than correlations in BOLD signals across regions over time. This means that the alignment measure described a feature of neural organization that was expressed in each measurement in time in each individual, rather than a second-order functional connectivity statistic. We found that across cognitive conditions the alignment measure was highly stable, operating as a trait-like variable. This indicates that the function–anatomy relationship is consistent within a person but variable between persons, and thus useful in examining individual variability in cognition.

With respect to recent dynamic network analyses of executive function, our results contribute a crucial anatomically grounded perspective. The current approach represents a framework in which to understand the dual features of anatomical organization and functional processes supporting cognitive flexibility in the human connectome. Here, high functional dependence in fronto-parietal, cingulo-opercular, default mode and subcortical systems is not associated with intersubject switching variability. Critically, our results indicate that regions that participate in highly flexible systems<sup>49</sup> in temporal network analysis demonstrate high dependence on underlying anatomical networks across frames of BOLD data during fixation, low cognitive control conditions and task conditions (see Supplementary Information for further analysis and discussion). Previous studies identify dynamic network roles for fronto-parietal and cingulo-opercular regions in cognitive switching, and our results indicate that moment-to-moment signal configurations in highly flexible systems are strongly organized by structure across time (see Supplementary Information for addition analysis and discussion). In the context of this highly organized cortical activity, the current results suggest that subcortical systems contain highly liberal signals. The extent to which subcortical systems exhibit relative alignment may form a flexible integrative role across the many computations supported by cortical systems. The relationship between anatomically bound momentary signal organization and functional reconfigurations in temporal networks may more generally provide an area for future research.

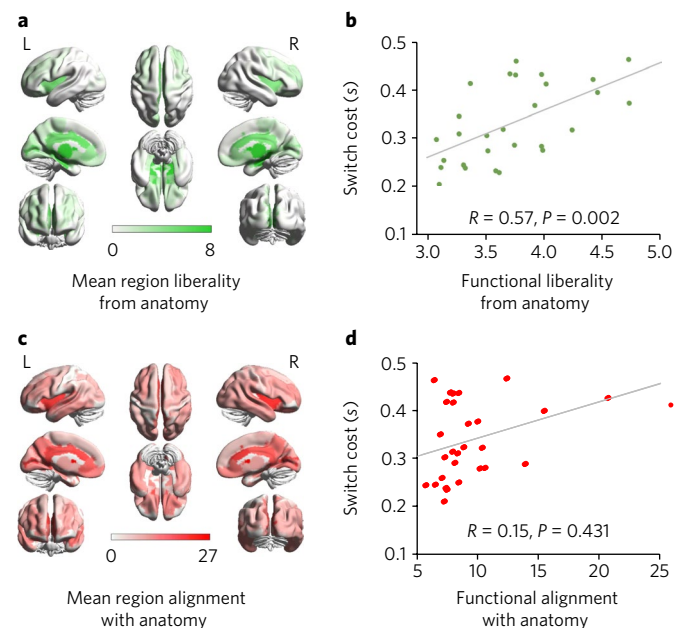


**Fig. 6 | Lower independence is associated with lower switch costs.**

**a**, For the 28 subjects, the liberal signals are concentrated especially in subcortical regions and cingulate cortices. **b**, Reduced liberality (increased alignment) is associated with reduced switch costs across subjects. **c**, Aligned signals are concentrated especially in subcortical, default mode, fronto-parietal and cingulo-opercular systems. **d**, Variability in aligned signals was not significantly associated with switch costs across subjects. In panels **a** and **c**, the coloured bars represent the GFT signal values at each region, where increasing values represent more liberality or alignment, respectively. In panels **b** and **d**, the x axes represent the mean liberality or alignment across regions of the brain, and the y axes represent the mean switch cost during the Navon task. L, left hemisphere; R, right hemisphere.

Notably, our results do not explain the potential cognitive role of highly aligned signals. We hypothesized that signal organization in the most liberal signals would be related to flexibility, representing the brain's dynamic freedom from anatomical constraints. It could also have been the case that relatively less alignment in the most aligned signals, representing modest dynamic freedom, was associated with greater flexibility. However, we did not observe this in the current data. It is possible that highly aligned signals are optimally configured in healthy brains. Important future directions could involve examining whether highly aligned signals are disrupted in clinical samples and associated with cognitive deficits.

It is possible that the role of aligned signals may be better explained in the context of other cognitive control processes<sup>50</sup>. One possible role for modestly aligned signals is to reduce noise when overcoming predisposed response tendencies for successful goal-directed behavioural switching. Specifically, subcortical structures maintain a high degree of signal alignment overall. Modest alignment of the most liberal signals in these same regions enable organized coordination across regions to facilitate switching. We speculate that anatomically aligned signals in fronto-parietal, cingulo-opercular, default mode and subcortical systems organize the dynamic signals contributing to cortical mechanisms of cognitive control, attention, and resting and preparedness processes, respectively. It would be interesting to test whether highly aligned signals in association cortices and subcortical structures are associated with domain-general performance variability across modalities<sup>51</sup>. In cognitive switching, specifically, the extent to which signal liberality relates to performance during tasks involving other sensory

modalities, transitioning between internally and externally focused attention and divergent thinking remains to be established. In addition, the relevance of liberal signals to cognitive flexibility may be further examined in populations with reduced performance, such as aging<sup>52</sup>, Gilles de la Tourette syndrome<sup>53</sup> and Parkinson's disease<sup>54</sup>.

Of note, the current study design establishes a correlative relationship between the neural measure of liberality and cognitive flexibility. Experiments that examine a causal relationship could provide important validation. Specifically, interventions involving medications that influence attention, behavioural training paradigms and noninvasive brain stimulation could examine whether BOLD signal alignment is sensitive to interventions and whether induced changes in liberal and aligned signals underlie changes in behaviour. Some promising mechanistic approaches involve a combination of biologically plausible models combined with fMRI and diffusion tractography, such as in dynamic causal modelling<sup>55</sup>. In addition, many approaches for diffusion tractography and parcellation are now available, although each has its strengths and limitations. Future studies that are focused on robust classification and prediction procedures could seek to further optimize network generation in these regards.

In conclusion, our results support the use of network science for clarifying mechanisms of executive function specifically and cognition more generally<sup>22,23</sup>. Recent literature firmly establishes that white matter organization is a critical, but incomplete determinant of functional signals in brain networks<sup>20,44–48</sup>. Conceptually, the current approach acknowledges that without structure, functional signals lack a mediating organization. By examining functional signal alignment within underlying white matter networks, we identify an important definition of dynamic contributions to cognitive switching that discriminates between the contributions of subcortical and other systems. Similar applications to other large multimodal neuroimaging datasets could contribute to biomarker analyses in psychiatric disease and neurological disorders, many of which are associated with deficits in executive function<sup>56–58</sup>.

## Methods

In this study, subjects performed a Navon switching task and Stroop inhibition task during fMRI scanning. We additionally acquired diffusion spectrum imaging data for white matter tractography. Within the Desikan–Killiany anatomical atlas<sup>49</sup> combined with the Harvard–Oxford subcortical parcels<sup>50</sup> and Diebridges cerebellar atlas<sup>27</sup>, we extracted preprocessed BOLD signals for each region for each time point. Then, we performed diffusion tractography and extracted an anatomical network in the same parcellation for each subject. To create the measure of BOLD signal alignment with underlying anatomical networks, we used tools from graph signal processing. Specifically, we treated observed BOLD vectors across regions at each time point as a signal on each subject's underlying anatomical graph. Then, we applied GFT to identify signals that were either highly aligned with the anatomical network or liberal with respect to the anatomical network for each subject. Across subjects, we calculated the correlation between the aligned (or liberal) signals and the behavioural variables of interest: in the Navon task, switch costs, which measure the time taken to perform a switch relative to a non-switch, and in the Stroop task, inhibition costs, which measure the time taken to respond to trials where cognitive inhibition is required relative to trials without inhibition demands.

**Subjects.** A total of 30 subjects were recruited. All subjects were screened for prior history of psychiatric or neurological illness. One subject was excluded due to near-chance performance on the task (accuracy = 52%). One additional subject was excluded due to technical problems on the day of scanning. The final sample included 28 individuals (mean age = 25.6, s.d. = 3.5, 70% Caucasian, 13 females). All subjects volunteered with informed consent in writing in accordance with the Institutional Review Board/Human Subjects Committee at the University of Pennsylvania.

**Behavioural task.** All participants completed a local–global perception task based on classical Navon figures<sup>55</sup>. Local–global stimuli consisted of four shapes—a circle, X, triangle or square—that were used to build the global and local aspects of the stimuli. In all trials, the local feature did not match the global feature, ensuring that subjects could not use information about one scale to infer information about another. Stimuli were presented on a black background in a block design with three block types (see Fig. 2). In the first block type, subjects viewed white local–global stimuli.

In the second block type, subjects viewed green local–global stimuli. In the third block type, stimuli switched between white and green across trials uniformly at random with the constraint that 70% of trials included a switch in each block. In all blocks, subjects were instructed to report only the local features of the stimuli if the stimulus was white, and to report only the global feature of the stimuli if the stimulus was green. Blocks were administered in a random order. Subjects responded using their right hand with a four-button box. All subjects were trained on the task outside the scanner until proficient at reporting responses using a fixed mapping between the shape and button presses (that is, index finger = circle, middle finger = X, ring finger = triangle, little finger = square). In the scanner, blocks were administered with 20 trials apiece separated by 20-s fixation periods with a white crosshair at the center of the screen. Each trial was presented for a fixed duration of 1,900 ms separated by an interstimulus interval of 100 ms during which time a black screen was presented.

**Diffusion spectrum imaging acquisition and processing.** Diffusion spectrum images were acquired on a Siemens 3.0T Tim Trio for all subjects along with a T1-weighted anatomical scan at each scanning session. We followed a parallel strategy for data acquisition and construction of streamline adjacency matrices as in previous work<sup>31,61</sup>. DSI scans sampled 257 directions using a Q5 half-shell acquisition scheme with a maximum *b*-value of 5,000 and an isotropic voxel size of 2.4 mm. We used an axial acquisition with the following parameters: repetition time (TR) = 5 s; echo time (TE) = 138 ms; 52 slices; field of view (FoV) = 231, 231, 125 mm. We acquired a three-dimensional SPGR T1 volume (TE = minimal full; flip angle = 15 degrees; FOV = 24 cm) for anatomical reconstruction. All subjects volunteered with informed consent in writing in accordance with the Institutional Review Board/Human Subjects Committee, University of Pennsylvania.

DSI data were reconstructed in DSI Studio ([www.dsi-studio.labsolver.org](http://www.dsi-studio.labsolver.org)) using *q*-space diffeomorphic reconstruction (QSDR)<sup>62</sup>. QSDR first reconstructs diffusion-weighted images in native space and computes the quantitative anisotropy (QA) in each voxel. These QA values are used to warp the brain to a template QA volume in Montreal Neurological Institute (MNI) space using the statistical parametric mapping (SPM) nonlinear registration algorithm. Once in MNI space, spin density functions were again reconstructed with a mean diffusion distance of 1.25 mm using three fibre orientations per voxel. Fibre tracking was performed in DSI studio with an angular cutoff of 35°, step size of 1.0 mm, minimum length of 10 mm, spin density function smoothing of 0.0, maximum length of 400 mm and a QA threshold determined by DWI signal in the colony-stimulating factor. Deterministic fibre tracking using a modified FACT algorithm was performed until 1,000,000 streamlines were reconstructed for each individual.

Anatomical scans were segmented using FreeSurfer<sup>53</sup> and parcellated using the connectome mapping toolkit<sup>56</sup>. A parcellation scheme including *n* = 129 regions was registered to the B0 volume from each subject's DSI data. The B0 to MNI voxel mapping produced via QSDR was used to map region labels from native space to MNI coordinates. To extend region labels through the grey–white matter interface, the atlas was dilated by 4 mm<sup>64</sup>. Dilatation was accomplished by filling non-labelled voxels with the statistical mode of their neighbours' labels. In the event of a tie, one of the modes was arbitrarily selected. Each streamline was labeled according to its terminal region pair.

Finally, we included a cerebellar parcellation<sup>27</sup>. We used FSL to nonlinearly register the individual's T1 to MNI space. Then, we used the inverse transform parameters to warp the cerebellum atlas to the individual T1. We registered the subject's DSI image to the T1. We used the inverse parameters from this registration to map the individualized cerebellar parcels into the subject's DSI space. Finally, we merged the cerebellar label image with the dilated cortical and subcortical parcellation image.

From these data and parcellation, we constructed an anatomical connectivity matrix, *A*, for which the element  $A_{ij}$  represented the number of streamlines connecting different regions<sup>20</sup>, divided by the sum of volumes for regions *i* and *j*<sup>55</sup>. Prior to data analysis, all cerebellum-to-cerebellum edges were removed from each individual's matrix, because cerebellar lobules are demonstrably not anatomically connected directly to one another<sup>66</sup>.

**Functional imaging acquisition and processing.** fMRI images were acquired during the same scanning session as the DSI data on a 3.0T Siemens Tim Trio whole-body scanner with a whole-head elliptical coil by means of a single-shot gradient-echo T2\* (TR = 1,500 ms; TE = 30 ms; flip angle = 60°; FoV = 19.2 cm; resolution 3 mm × 3 mm × 3 mm). Preprocessing was performed using FEAT (fMRI expert analysis tool) v.6.0 a component of the FSL software package<sup>67</sup>. To prepare the functional images for analyses, we completed the following steps: skull-stripping with BET to remove non-brain material, motion correction with MCFLIRT (FMRIB's linear image registration tool)<sup>67</sup>, slice-timing correction (interleaved), spatial smoothing with a 6-mm 3D Gaussian kernel and high-pass temporal filtering to reduce low frequency artifacts. We also performed EPI unwarping with fieldmaps in order to improve subject registration to standard space. Native image transformation to a standard template was completed using FSL's affine registration tool, FLIRT<sup>67</sup>. Subject-specific functional images were co-registered to their corresponding high-resolution anatomical images via a boundary based registration (BBR)<sup>68</sup> technique and were then registered to the

standard MNI-152 structural template via a 12-parameter linear transformation. Finally, each participant's individual anatomical image was segmented into grey matter, white matter and cerebrospinal fluid (CSF) using the binary segmentation function of FAST (FMRIB's automated segmentation tool)<sup>69</sup> v.4.0. The white matter and CSF masks for each participant were then transformed to native functional space and the average time series were extracted. Images were spatially smoothed using a kernel with a full-width at half-maximum of 6 mm. These values were used as confound regressors on our time series along with 18 translation and rotation parameters as estimated by MCFLIRT<sup>70</sup>.

**Functional decomposition into anatomical networks.** To investigate our hypothesis that BOLD signal alignment with anatomy is related to cognitive flexibility, we applied an analysis from spectral graph theory<sup>71</sup>. Specifically, we used GFT<sup>28</sup> to represent the BOLD signals in the graph domain. This allowed us to take observed BOLD time series and examine the extent to which they were aligned to or liberal from the underlying graph representing the white matter connections between regions.

The approach differed from structure–function analyses of pairwise relationships between anatomical and functional network connections<sup>20,44–48</sup>. The GFT provided a distinct perspective from connectivity analyses by allowing the spectrum of the entire anatomical matrix to inform estimates of how BOLD signals in each observation (not functional connections computed over time) align with white matter. Importantly, each element (region) in either the aligned or liberal BOLD signal vector represented the extent to which that region conformed to or deviated from the expected signal with respect to the topology of the entire white matter network, rather than with respect to single anatomical connections.

An important conceptual benefit of the GFT is that it could be used to study how the topology of an individual's anatomical network informed the expected structure of the BOLD signal. We assessed the deviation of the BOLD signal from this expectation at each moment in time, as opposed to an average over all moments in time, which provides inherently limited information<sup>39</sup>. The approach thus used functional measurements that are commonly used to construct functional graphs, and examined their expression atop anatomy in single individuals. Another important benefit of the GFT is that it allowed us to treat signal alignment and liberality as related phenomena that are not mutually exclusive from one another. Intuitively, this can be understood by analogy to Fourier analysis in the time domain, where a time series can be transformed into the frequency domain such that its high and low frequency content can be studied. Similarly, GFT can be used to transform a vector of BOLD magnitudes at a single TR into aligned and liberal portions with respect to the anatomical network. The aligned and liberal signals are directly analogous to low and high frequencies in traditional Fourier analysis, and are, as such, not mutually exclusive. Thus, the GFT allowed us to consider the amount of signal that was aligned and liberal with respect to the graph. Only if the signal was perfectly aligned or unaligned with the graph would we expect the transformed signals to exhibit nonzero quantities of both signal characteristics. This is analogous to expecting any natural signal in the time domain to represent frequency domain content that exceeds a single frequency.

Conceptually, there was no initial analytic constraint on where the aligned and liberal signals most prominently exist in the brain; indeed, it was possible that they may have overlapped in the same regions of the brain. This too can be understood by analogy to traditional time–frequency analysis using the Fourier transform. A priori, each moment in time in a Fourier transformation contributes to the transformed time–frequency representation of the data, including both high and low frequency activity. Analogously, regions across the brain expressed BOLD signals that contribute to both aligned and liberal signals that are separated by the GFT. This allowed us to detect which specific nodes are contributing most to aligned and liberal signals, and we could empirically determine to what extent the aligned and liberal signals overlapped in the brain. See Fig. 4 for a schematic illustrating the analogy between signal frequency in the time domain and signal alignment in the graph domain.

It is important to note that the ranges of aligned and liberal signals are extremes along a continuum of alignment selected to be robust to noise. We use the terms aligned and liberal to categorically refer to each extreme. Critically, it is the case that increasing alignment does not imply decreasing liberality, because these refer to two distinct ranges in the graph signal. This is because our selection of aligned and liberal signals is analogous to selecting the high and low frequency ranges of a signal in traditional Fourier transformation. For example, if we used a traditional Fourier transformation on a full time series and selected only frequencies of 1–10 Hz and 90–100 Hz in the time–frequency domain, shifts from 1 to 10 Hz would represent increasing frequency, but would still be represented in the 1–10 Hz range. Similarly, shifts from 100 to 90 Hz would represent decreasing frequency. However, it is not necessarily the case that shifts in the 1–10 Hz range are associated with changes in the 90–100 Hz range and vice versa. Thus, it is sensible to speak about both ranges separately, and it is not necessarily the case that they correlate with one another. To determine whether they are correlated with one another, the presence and variability at each end of the spectrum must be empirically investigated in a natural system.

It is crucial to clarify the biological and cognitive relevance of the alignment/liberality measure. Biologically, the measure described the deviation of the BOLD signal organization across the brain at each time point with respect to its underlying anatomy. This is interesting because we might assume on the one hand that cognitive function must to some extent depend on underlying anatomy to organize signal processes, but on the other hand that some cognitive processes may benefit from deviating from this anatomy. Here, we anticipated that the most liberal signals would be sensitive to variability in switch costs, because these are the signals that most highly deviate from underlying white matter network organization. Intuitively, these signals were those that may facilitate rapid cognitive switches based on a recently learned rule, because the rules cannot be represented in the connecting white matter pathways reconstructed by our diffusion tractography. Our method identified the spatial distribution and intensity of the aligned and liberal signals so that we could test for the behaviourally relevant components of BOLD signal organization in subject-specific white matter networks.

We then proceeded to the technical definition of our alignment and liberality measures. We analysed the signal defined on a connected, weighted and symmetric graph,  $G = (V, A)$ , where  $V = \{1, \dots, n\}$  is a set of  $n$  vertices or nodes representing individual brain regions and  $A \in R^{n \times n}$  is defined as above. Because the network  $A$  was symmetric, it had a complete set of orthonormal eigenvectors associated with it<sup>28,71</sup>. For this reason, it had an eigenvector decomposition,  $A = V\Lambda V^T$ , in which  $\Lambda$  was the set of eigenvalues, ordered so that  $\lambda_0 \leq \lambda_1 \leq \dots \leq \lambda_{n-1}$ , and  $V = \{v_k\}_{k=0}^{n-1}$  was the set of associated eigenvectors. Following refs<sup>28,72</sup>, we used the eigenvector matrix to define the GFT of the graph signal  $x \in R^n$  as

$$\tilde{x} = v^T x \quad (1)$$

Given  $\tilde{x} = [\tilde{x}_0, \dots, \tilde{x}_{n-1}]^T$ , we could express the original signal as  $x = \sum_{k=0}^{n-1} \tilde{x}_k v_k$ , a sum of the eigenvector components  $v_k$ . The contribution of  $v_k$  to signal  $x$  was the GFT component  $\tilde{x}_k$ . Note that the smoothness of  $v_k$  on the network can be evaluated in the quadratic form  $v_k^T A v_k = \sum_{i,j \in V} A_{ij} v_k(i) v_k(j)$  and that  $v_k^T A v_k = \lambda_k$  is given by the eigenvector decomposition. The quantity  $\sum_{i,j \in V} A_{ij} v_k(i) v_k(j)$  will be negative when the signal is varied (highly connected regions possess signals of different signs), and positive when the signal is smooth (highly connected regions possess signals of same signs). For these reasons, this quantity can be thought of as a measure of smoothness (alignment). Consequently, the GFT coefficients  $\tilde{x}_k$  for small values of  $k$  indicated how much variables that are highly misaligned (liberality) with anatomy contribute to the observed brain signal  $x$ . GFT coefficients  $\tilde{x}_k$  for large values of  $k$  described how much signals that were aligned with the anatomical network contributed to the observed brain signal  $x$ . The inverse (i) GFT of  $\tilde{x}$  with respect to  $A$  was defined as

$$x = \tilde{V}\tilde{x} \quad (2)$$

Given a graph signal  $x$  with GFT  $\tilde{x}$ , we could isolate the liberal components corresponding to the lowest  $K_L$  eigenvectors by applying a graph filter  $H_L$  that only kept components with  $k < K_L$  and sets other components to 0. The signal  $x_L$  then contained the liberal components of  $x$  (those with a low alignment with network anatomy). Apart from the graph low-pass filter  $H_L$ , we also considered a middle graph regime  $H_M$ , which kept only components in the range of  $K_L \leq k < K_A$ , and an aligned graph regime  $H_A$ , such that only network-aligned components with  $n - K_A \leq k$  were kept. Therefore, the liberal regime took the lowest  $K_L$  components, the alignment regime took the highest  $K_A$  components, and the middle regime captured the middle  $n - K_L - K_M$  components (here, we used the components with the 10 lowest alignment values to represent the liberal regime and the components with the 10 highest alignment values to represent the aligned regime; see Supplementary Information for robustness of results to parameter selection). Because we used  $x_L$  and  $x_A$  to respectively denote the signals represented by the middle and highly aligned regimes, the original signal could be written as the sum  $x = x_L + x_M + x_A$ . This formulation gave a decomposition of the original signals  $x$  into liberal, moderately aligned and highly aligned components that respectively represented signals that had high, medium and low signal deviation with respect to the anatomical connectivity between brain regions.

Previous studies have consistently demonstrated that the aligned and liberal components aid in better estimation of unknown movie ratings in recommendation systems<sup>73</sup>, better prediction of cancer using gene interaction networks<sup>74,75</sup> and learning in neuroimaging data, where learning-related processes are demonstrably expressed in low and high components in fMRI data, and where the middle component  $x_M$  is demonstrably less reliable and behaviourally uninformative<sup>76</sup>. In the Supplementary Information, we perform a similar analysis to data from ref.<sup>76</sup>, but with the current data to examine the stability of our low and high alignment measurements to parameter selection. The data indicate that the low and high alignment components in the current data are stable. Mathematically, this is expected in general for applications of the current approach, because eigenvalues at the extreme low and high end are isolated from the middle values, which leads to robustness in the high and low ranges of the decomposition<sup>77</sup>.

We note that this approach allowed signals on the anatomical network to contain both aligned and liberal components represented in the same region at a single TR. This feature occurred because the anatomical network of  $n$  nodes has  $n^2$  entries (that is, the connection information was encoded in the anatomical adjacency matrix for any node  $i$  to any node  $j$ ). Rather than examining a single BOLD signal measurement as  $n$  independently observed values, the GFT represented the signal to be a composite of contributions to the signal across subject's anatomical network topology. The decomposition occurred across the entire set of signals (here, the vector of BOLD magnitudes across regions at a single TR), where there are only  $n$  entries. The GFT applied here leverages the fact that the  $n$  entries in a given vector are not isolated, but are signals on top of the complex anatomical network. In the current approach, instead of focusing on the single BOLD value observed at each region as a discrete entity, the decomposition was sensitive to the observation of pairwise differences among BOLD signals relative to those expected by the anatomical network. A proportion of each given region's BOLD signal was estimated to be liberal with respect to the network, which was represented by  $x_l$ , and a proportion was estimated to be aligned with the network, which was represented by  $x_a$  (see Fig. 3). This mathematical separation established the notions of alignment and liberality of the BOLD signals in the anatomical network. All individual regions in the brain could have some degree of alignment and some degree of liberality given the complexity of BOLD signal patterns across the network, unless the observed BOLD signals in all regions were perfectly aligned or perfectly misaligned with the subject's anatomical network. This highlights an important strength of the use of GFT to examine functional signal liberality in anatomical brain networks: in general, the signal can be understood as a network level composite of aligned and liberal signals, and the extent to which individual regions contribute to these properties can be examined as the variation in the weights of the region's contribution to each of the aligned and liberal components.

**Relating signals to behaviour.** Following the signal decomposition into aligned and liberal signals, we associated the signal concentrations with median switch cost (median response time during switching trials versus no-switching trials) performance for all accurate trials. To do so, we computed a partial Pearson's correlation between the observed signal value for each subject and their median switch cost using the average framewise displacement across BOLD measurements as a second-level control for the influences of motion. Specifically, to examine the relationship between alignment and switch costs across subjects, we computed the partial correlation for the mean of  $x_a$  for each subject with subjects' switch costs, controlling for average framewise displacement. Then, to examine the relationship between liberality and switch costs, across subjects, we computed the partial correlation for the mean of  $x_l$  for each subject with subjects' switch costs, controlling for average framewise displacement. We additionally repeated these analyses including age and sex, and found similar slopes for the associations between the liberality values and switch costs (see Supplementary Information).

**System permutation test.** To examine the spatial significance of system-level concentration of aligned and liberal signals, we performed a non-parametric permutation test for each signal class. For each  $x_l$  and  $x_a$  separately, we shuffled the observed mean signal concentration values across regions in 10,000 permutations for aligned and liberal signals and computed a null distribution of system mean signal concentrations for each system. Signals were judged to be significantly concentrated in a system if the mean signal concentration in the system was greater or less than 95% of the null permutations.

**Life Sciences Reporting Summary.** Further information on experimental design is available in the Life Sciences Reporting Summary.

**Code availability.** Requests for code can be addressed to the corresponding author.

**Data availability.** Requests for data can be addressed to the corresponding author.

Received: 8 December 2016; Accepted: 7 November 2017;

Published online: 18 December 2017

## References

- Rogers, R. D. & Monsell, S. Costs of a predictable switch between simple cognitive tasks. *J. Exp. Psychol. Gen.* **124**, 207–231 (1995).
- Szczepanski, S. M. & Knight, R. T. Insights into human behavior from lesions to the prefrontal cortex. *Neuron* **83**, 1002–1018 (2014).
- Clark, L. R. et al. Specific measures of executive function predict cognitive decline in older adults. *J. Int. Neuropsychol. Soc.* **18**, 118–127 (2012).
- Richland, L. E. & Burchinal, M. R. Early executive function predicts reasoning development. *Psychol. Sci.* **24**, 87–92 (2013).
- Davis, J. C., Marra, C. A., Najafzadeh, M. & Liu-Ambrose, T. The independent contribution of executive functions to health related quality of life in older women. *BMC Geriatr.* **10**, 16 (2010).
- Gunaydin, L. A. & Kreitzer, A. C. Cortico-basal ganglia circuit function in psychiatric disease. *Annu. Rev. Physiol.* **78**, 327–350 (2016).
- Casey, B. et al. Early development of subcortical regions involved in non-cued attention switching. *Dev. Sci.* **7**, 534–542 (2004).
- Cole, M. W. et al. Multi-task connectivity reveals flexible hubs for adaptive task control. *Nat. Neurosci.* **16**, 1348–1355 (2013).
- Heyder, K., Suchan, B. & Daum, I. Cortico-subcortical contributions to executive control. *Acta Psychol.* **115**, 271–289 (2004).
- Luk, G., Green, D. W., Abutalebi, J. & Grady, C. Cognitive control for language switching in bilinguals: a quantitative meta-analysis of functional neuroimaging studies. *Lang. Cogn. Process.* **27**, 1479–1488 (2012).
- Quilodran, R., Rothe, M. & Procyk, E. Behavioral shifts and action valuation in the anterior cingulate cortex. *Neuron* **57**, 314–325 (2008).
- Ridderinkhof, K. R., Van Den Wildenberg, W. P., Segalowitz, S. J. & Carter, C. S. Neurocognitive mechanisms of cognitive control: the role of prefrontal cortex in action selection, response inhibition, performance monitoring, and reward-based learning. *Brain Cogn.* **56**, 129–140 (2004).
- Esterman, M., Chiu, Y.-C., Tammer-Rosenau, B. J. & Yantis, S. Decoding cognitive control in human parietal cortex. *Proc. Natl Acad. Sci. USA* **106**, 17974–17979 (2009).
- Hikosaka, O. & Isoda, M. Switching from automatic to controlled behavior: cortico-basal ganglia mechanisms. *Trends Cogn. Sci.* **14**, 154–161 (2010).
- Hosoda, C., Hanakawa, T., Nariai, T., Ohno, K. & Honda, M. Neural mechanisms of language switch. *J. Neurolinguist.* **25**, 44–61 (2012).
- Leunissen, J. et al. Subcortical volume analysis in traumatic brain injury: the importance of the fronto-striato-thalamic circuit in task switching. *Cortex* **51**, 67–81 (2014).
- Yehene, E., Meiran, N. & Soroker, N. Basal ganglia play a unique role in task switching within the frontal-subcortical circuits: evidence from patients with focal lesions. *J. Cogn. Neurosci.* **20**, 1079–1093 (2008).
- Sporns, O., Tononi, G. & Kötter, R. The human connectome: a structural description of the human brain. *PLoS Comput. Biol.* **1**, e42 (2005).
- Alstott, J., Breakspear, M., Hagmann, P., Cammoun, L. & Sporns, O. Modeling the impact of lesions in the human brain. *PLoS Comput. Biol.* **5**, e1000408 (2009).
- Hermundstad, A. M. et al. Structural foundations of resting-state and task-based functional connectivity in the human brain. *Proc. Natl Acad. Sci. USA* **110**, 6169–6174 (2013).
- Honey, C. J., Kötter, R., Breakspear, M. & Sporns, O. Network structure of cerebral cortex shapes functional connectivity on multiple time scales. *Proc. Natl Acad. Sci. USA* **104**, 10240–10245 (2007).
- Medaglia, J. D., Lynall, M.-E. & Bassett, D. S. Cognitive network neuroscience. *J. Cogn. Neurosci.* **27**, 1471–1491 (2015).
- Sporns, O. Contributions and challenges for network models in cognitive neuroscience. *Nat. Neurosci.* **17**, 652–660 (2014).
- Power, J. D. et al. Functional network organization of the human brain. *Neuron* **72**, 665–678 (2011).
- Navon, D. Forest before trees: the precedence of global features in visual perception. *Cognit. Psychol.* **9**, 353–383 (1977).
- Cammoun, L. et al. Mapping the human connectome at multiple scales with diffusion spectrum MRI. *J. Neurosci. Methods* **203**, 386–397 (2012).
- Diedrichsen, J., Balsters, J. H., Flavell, J., Cussans, E. & Ramnani, N. A probabilistic MR atlas of the human cerebellum. *Neuroimage* **46**, 39–46 (2009).
- Sandryhaila, A. & Moura, J. M. Discrete signal processing on graphs. *IEEE Trans. Signal Process.* **61**, 1644–1656 (2013).
- Braver, T. S. The variable nature of cognitive control: a dual mechanisms framework. *Trends Cogn. Sci.* **16**, 106–113 (2012).
- Botvinick, M. & Braver, T. Motivation and cognitive control: from behavior to neural mechanism. *Annu. Rev. Psychol.* **66**, 83–113 (2015).
- Gu, S. et al. Controllability of structural brain networks. *Nat. Commun.* **6**, 8414 (2015).
- Cohen, J. D., Dunbar, K. & McClelland, J. L. On the control of automatic processes: a parallel distributed processing account of the Stroop effect. *Psychol. Rev.* **97**, 332–361 (1990).
- Zatorre, R. J., Fields, R. D. & Johansen-Berg, H. Plasticity in gray and white: neuroimaging changes in brain structure during learning. *Nat. Neurosci.* **15**, 528–536 (2012).
- Li, P., Legault, J. & Litcofsky, K. A. Neuroplasticity as a function of second language learning: anatomical changes in the human brain. *Cortex* **58**, 301–324 (2014).
- Wang, X., Casadio, M., Weber, K. A., Mussa-Ivaldi, F. A. & Parrish, T. B. White matter microstructure changes induced by motor skill learning utilizing a body machine interface. *Neuroimage* **88**, 32–40 (2014).
- Reid, L. B., Sale, M. V., Cunningham, R., Mattingley, J. B. & Rose, S. E. Brain changes following four weeks of unimanual motor training: evidence from fMRI-guided diffusion MRI tractography. *Hum. Brain Mapp.* **38**, 4302–4312 (2017).
- Braun, U. et al. Dynamic reconfiguration of frontal brain networks during executive cognition in humans. *Proc. Natl Acad. Sci. USA* **112**, 11678–11683 (2015).

38. Mayhew, S. D. et al. Global signal modulation of single-trial fMRI response variability: effect on positive vs negative bold response relationship. *Neuroimage* **133**, 62–74 (2016).
39. Marrelec, G., Messé, A., Giron, A. & Rudrauf, D. Functional connectivity's degenerate view of brain computation. *PLoS Comput. Biol.* **12**, e1005031 (2016).
40. Sekutowicz, M. et al. Striatal activation as a neural link between cognitive and perceptual flexibility. *Neuroimage* **141**, 393–398 (2016).
41. Liston, C., Matalon, S., Hare, T. A., Davidson, M. C. & Casey, B. Anterior cingulate and posterior parietal cortices are sensitive to dissociable forms of conflict in a task-switching paradigm. *Neuron* **50**, 643–653 (2006).
42. Peltig, D. P., Pakkenberg, H., Stark, A. K. & Pakkenberg, B. Neocortical glial cell numbers in human brains. *Neurobiol. Aging* **29**, 1754–1762 (2008).
43. Middleton, F. A. & Strick, P. L. Anatomical evidence for cerebellar and basal ganglia involvement in higher cognitive function. *Science* **266**, 458–461 (1994).
44. Greicius, M. D., Supekar, K., Menon, V. & Dougherty, R. F. Resting-state functional connectivity reflects structural connectivity in the default mode network. *Cereb. Cortex* **19**, 72–78 (2009).
45. Hermundstad, A. M. et al. Structurally-constrained relationships between cognitive states in the human brain. *PLoS Comput. Biol.* **10**, e1003591 (2014).
46. Honey, C. et al. Predicting human resting-state functional connectivity from structural connectivity. *Proc. Natl Acad. Sci. USA* **106**, 2035–2040 (2009).
47. Morgan, V. L., Mishra, A., Newton, A. T., Gore, J. C. & Ding, Z. Integrating functional and diffusion magnetic resonance imaging for analysis of structure–function relationship in the human language network. *PLoS ONE* **4**, e6660 (2009).
48. Uddin, L. Q., Supek, K. S., Ryali, S. & Menon, V. Dynamic reconfiguration of structural and functional connectivity across core neurocognitive brain networks with development. *J. Neurosci.* **31**, 18578–18589 (2011).
49. Mattar, M. G., Betzel, R. F. & Bassett, D. S. The flexible brain. *Brain* **139**, 2110–2112 (2016).
50. Miyake, A. et al. The unity and diversity of executive functions and their contributions to complex “frontal lobe” tasks: a latent variable analysis. *Cognit. Psychol.* **41**, 49–100 (2000).
51. Fedorenko, E. The role of domain-general cognitive control in language comprehension. *Front. Psychol.* **5**, 335 (2014).
52. Gajewski, P. D. et al. Effects of aging and job demands on cognitive flexibility assessed by task switching. *Biol. Psychol.* **85**, 187–199 (2010).
53. Eddy, C. M., Rizzo, R. & Cavanna, A. E. Neuropsychological aspects of Tourette syndrome: a review. *J. Psychosom. Res.* **67**, 503–513 (2009).
54. Cools, R., Barker, R. A., Sahakian, B. J. & Robbins, T. W. Enhanced or impaired cognitive function in Parkinson's disease as a function of dopaminergic medication and task demands. *Cereb. Cortex* **11**, 1136–1143 (2001).
55. Stephan, K. E., Tittgemeyer, M., Knösche, T. R., Moran, R. J. & Friston, K. J. Tractography-based priors for dynamic causal models. *Neuroimage* **47**, 1628–1638 (2009).
56. Belleville, S., Bherer, L., Lepage, É., Chertkow, H. & Gauthier, S. Task switching capacities in persons with Alzheimer's disease and mild cognitive impairment. *Neuropsychologia* **46**, 2225–2233 (2008).
57. Kehagia, A. A., Barker, R. A. & Robbins, T. W. Neuropsychological and clinical heterogeneity of cognitive impairment and dementia in patients with Parkinson's disease. *Lancet Neurol.* **9**, 1200–1213 (2010).
58. Kinnunen, K. M. et al. White matter damage and cognitive impairment after traumatic brain injury. *Brain* **134**, 449–463 (2011).
59. Desikan, R. S. et al. An automated labeling system for subdividing the human cerebral cortex on MRI scans into gyral based regions of interest. *Neuroimage* **31**, 968–980 (2006).
60. Kennedy, D. et al. Gyri of the human neocortex: an MRI-based analysis of volume and variance. *Cereb. Cortex* **8**, 372–384 (1998).
61. Betzel, R. F., Gu, S., Medaglia, J. D., Pasqualetti, F. & Bassett, D. S. Optimally controlling the human connectome: the role of network topology. *Sci. Rep.* **6**, 30770 (2016).
62. Yeh, F.-C., Wedeen, V. J. & Tseng, W.-Y. I. Estimation of fiber orientation and spin density distribution by diffusion deconvolution. *Neuroimage* **55**, 1054–1062 (2011).
63. Fischl, B. Freesurfer. *Neuroimage* **62**, 774–781 (2012).
64. Cieslak, M. & Grafton, S. Local termination pattern analysis: a tool for comparing white matter morphology. *Brain Imaging Behav.* **8**, 292–299 (2014).
65. Hagmann, P. et al. Mapping the structural core of human cerebral cortex. *PLoS. Biol.* **6**, e159 (2008).
66. Voogd, J. & Glickstein, M. The anatomy of the cerebellum. *Trends Cogn. Sci.* **2**, 307–313 (1998).
67. Jenkinson, M., Beckmann, C. F., Behrens, T. E., Woolrich, M. W. & Smith, S. M. Fsl. *Neuroimage* **62**, 782–790 (2012).
68. Greve, D. N. & Fischl, B. Accurate and robust brain image alignment using boundary-based registration. *Neuroimage* **48**, 63–72 (2009).
69. Zhang, Y., Brady, M. & Smith, S. Segmentation of brain MR images through a hidden Markov random field model and the expectation–maximization algorithm. *IEEE Trans. Med. Imaging* **20**, 45–57 (2001).
70. Jenkinson, M., Bannister, P., Brady, M. & Smith, S. Improved optimization for the robust and accurate linear registration and motion correction of brain images. *Neuroimage* **17**, 825–841 (2002).
71. Chung, F. R. K. *Spectral Graph Theory* Vol. 92 (American Mathematical Soc., 1997).
72. Shuman, D. I., Narang, S. K., Frossard, P., Ortega, A. & Vandergheynst, P. The emerging field of signal processing on graphs: extending high-dimensional data analysis to networks and other irregular domains. *IEEE Signal Process. Mag.* **30**, 83–98 (2013).
73. Ma, J., Huang, W., Segarra, S. & Ribeiro, A. Diffusion filtering for graph signals and its use in recommendation systems. In *IEEE Int. Conf. on Acoustics, Speech and Signal Processing* 4563–4567 (Shanghai, 2016).
74. Segarra, S., Huang, W. & Ribeiro, A. Diffusion and superposition distances for signals supported on networks. *IEEE Trans. Signal Inform. Process. Network* **1**, 20–32 (2015).
75. Huang, W., Segarra, S. & Ribeiro, A. Diffusion distance for signals supported on networks. In *Proc. Asilomar Conf. Signals Syst. Comput.* 1219–1223 (Asilomar, CA, 2015).
76. Huang, W. et al. Graph frequency analysis of brain signals. *IEEE J. Sel. Top. Signal Process.* **10**, 1189–1203 (2016).
77. Spielman, D. Spectral graph theory and its applications. In *48th Annual IEEE Symposium on Foundations of Computer Science, 2007. FOCS'07* 29–38 (2007).

## Acknowledgements

J.D.M. acknowledges support from the Office of the Director at the National Institutes of Health through grant number 1-DP5-OD-021352-01 and the Perleman School of Medicine. D.S.B. acknowledges support from the John D. and Catherine T. MacArthur Foundation, the Alfred P. Sloan Foundation, the Army Research Laboratory and the Army Research Office through contract numbers W911NF-10-2-0022 and W911NF-14-1-0679, the National Institute of Health (R01-DC-009209-11, R01-HD-086888-01, R01-MH-107235, R01-MH107703, R01-MH-109520, R01-NS-099348 and R21-MH-106799), the Office of Naval Research and the National Science Foundation (BCS-1441502, CAREER PHY-1554488, BCS-1631550, and CNS-1626008). The content is solely the responsibility of the authors and does not necessarily represent the official views of any of the funding agencies. The funders had no role in study design, data collection and analysis, decision to publish, or preparation of the manuscript.

## Author contributions

J.D.M. conceptualized the overall project, created the behavioural tasks, collected the data, wrote the manuscript and conducted behavioural and network data processing and analyses. W.H. performed primary analyses using GFT to integrate BOLD fMRI data with anatomical networks and to correlate them with cognitive measures. E.A.K. preprocessed BOLD fMRI data. A.K. adapted processing procedures to analyse the Human Connectome Project data. S.L.T.-S. assisted with the behavioural task design. A.R. supervised applications of the GFT analysis to the imaging data. D.S.B. funded the data acquisition, assisted with the interpretation of the primary findings and edited the manuscript.

## Competing interests

The authors declare no competing interests.

## Additional information

**Supplementary information** is available for this paper at <https://doi.org/10.1038/s41562-017-0260-9>.

**Reprints and permissions information** is available at [www.nature.com/reprints](http://www.nature.com/reprints).

**Correspondence and requests for materials** should be addressed to D.S.B.

**Publisher's note:** Springer Nature remains neutral with regard to jurisdictional claims in published maps and institutional affiliations.

Corresponding author(s): Danielle S. Bassett, Ph.D.

 Initial submission    Revised version    Final submission

## Life Sciences Reporting Summary

Nature Research wishes to improve the reproducibility of the work that we publish. This form is intended for publication with all accepted life science papers and provides structure for consistency and transparency in reporting. Every life science submission will use this form; some list items might not apply to an individual manuscript, but all fields must be completed for clarity.

For further information on the points included in this form, see [Reporting Life Sciences Research](#). For further information on Nature Research policies, including our [data availability policy](#), see [Authors & Referees](#) and the [Editorial Policy Checklist](#).

### ► Experimental design

#### 1. Sample size

Describe how sample size was determined.

The sample size chosen was selected to exceed that of recent hypothesis-driven fMRI or DSI-based network analyses, which can involve as few as 8 subjects in some recent prominent work. We chose to initially recruit 30 subjects to obtain better estimates for effect sizes and variances in the current study.

#### 2. Data exclusions

Describe any data exclusions.

One subject was excluded due to near-chance performance on the task (accuracy = 52%). One additional subject was excluded due to technical problems on the day of scanning. These criteria were chosen ahead of time: subjects less than 70% accuracy are typically excluded in our research because they make it unclear whether subjects can actually understand the tasks, and incomplete data due to technical failure is generally excluded from analysis.

#### 3. Replication

Describe whether the experimental findings were reliably reproduced.

We collected one moderately sized sample for the current study and conducted all analyses within this group. We decided to select a sufficient sample size to benchmark this analysis because it has not been conducted previously. A matching comparison sample was not feasible to collect given funding constraints. For quality assurance in the current analyses, the first author and second author each independently computed the primary results in the manuscript prior to the first submission and again after receiving the first reviews. We provide sufficient detail in the manuscript and data and code availability upon request if others would like to replicate analyses.

#### 4. Randomization

Describe how samples/organisms/participants were allocated into experimental groups.

Healthy adults above the age of 18 were recruited in the current study and each participated in a uniform research design with randomized stimulus blocks.

#### 5. Blinding

Describe whether the investigators were blinded to group allocation during data collection and/or analysis.

Blinding was not relevant because all subjects participated in an identical research design.

Note: all studies involving animals and/or human research participants must disclose whether blinding and randomization were used.

## 6. Statistical parameters

For all figures and tables that use statistical methods, confirm that the following items are present in relevant figure legends (or in the Methods section if additional space is needed).

n/a Confirmed

- The exact sample size (*n*) for each experimental group/condition, given as a discrete number and unit of measurement (animals, litters, cultures, etc.)
- A description of how samples were collected, noting whether measurements were taken from distinct samples or whether the same sample was measured repeatedly
- A statement indicating how many times each experiment was replicated
- The statistical test(s) used and whether they are one- or two-sided (note: only common tests should be described solely by name; more complex techniques should be described in the Methods section)
- A description of any assumptions or corrections, such as an adjustment for multiple comparisons
- The test results (e.g. *P* values) given as exact values whenever possible and with confidence intervals noted
- A clear description of statistics including central tendency (e.g. median, mean) and variation (e.g. standard deviation, interquartile range)
- Clearly defined error bars

See the web collection on [statistics for biologists](#) for further resources and guidance.

## ► Software

Policy information about [availability of computer code](#)

### 7. Software

Describe the software used to analyze the data in this study.

fMRI data were preprocessed in the FMRIB Software Library (FSL). DSI data were processed in DSI-studio. Graph Fourier Transformations were computed using custom Matlab code.

For manuscripts utilizing custom algorithms or software that are central to the paper but not yet described in the published literature, software must be made available to editors and reviewers upon request. We strongly encourage code deposition in a community repository (e.g. GitHub). [Nature Methods guidance for providing algorithms and software for publication](#) provides further information on this topic.

## ► Materials and reagents

Policy information about [availability of materials](#)

### 8. Materials availability

Indicate whether there are restrictions on availability of unique materials or if these materials are only available for distribution by a for-profit company.

Data were collected on an Army Research Laboratory grant awarded to the corresponding author and are available upon request.

### 9. Antibodies

Describe the antibodies used and how they were validated for use in the system under study (i.e. assay and species).

Not applicable.

### 10. Eukaryotic cell lines

a. State the source of each eukaryotic cell line used.

Not applicable.

b. Describe the method of cell line authentication used.

Not applicable.

c. Report whether the cell lines were tested for mycoplasma contamination.

Not applicable.

d. If any of the cell lines used are listed in the database of commonly misidentified cell lines maintained by [ICLAC](#), provide a scientific rationale for their use.

Provide a rationale for the use of commonly misidentified cell lines OR state that no commonly misidentified cell lines were used.

## ► Animals and human research participants

Policy information about [studies involving animals](#); when reporting animal research, follow the [ARRIVE guidelines](#)

### 11. Description of research animals

Provide details on animals and/or animal-derived materials used in the study.

Not applicable.

Policy information about [studies involving human research participants](#)

12. Description of human research participants

Describe the covariate-relevant population characteristics of the human research participants.

The final sample included 28 individuals (mean age = 25.6, St.D. = 3.5, 70% Caucasian, 13 females).